Supporting Information

Padovani et al. 10.1073/pnas.1409832111

SI Experimental Procedures

Expression and Purification of Recombinant Proteins. Human EFA6A^{Sec7} (residues 527–727) and EFA6A$^{Sec7\text{-}PH\text{-}Ct}$ (residues 527–1024) were cloned into a pProEX HTb plasmid with an N-terminal 6-His tag and tobacco etch virus (TEV) protease cleavage site. Both constructs were overexpressed in *Escherichia coli* and purified essentially as described previously for EFA6A$^{Sec7\text{-}PH\text{-}Ct}$ (1), except that the 6-His tag was removed by TEV protease treatment (1 mg TEV/10 mg proteins, overnight at 4 °C) before the ion-exchange chromatography step.

Different vectors were used for EFA6A$^{PH\text{-}Ct}$ (residues 730–1024). For use in nucleotide exchange experiments, EFA6A$^{PH\text{-}Ct}$ with an N-terminal 6-His tag was cloned into pET8C (Novagen) and purified by affinity chromatography on a HisTrap FF column, followed by ion-exchange chromatography on a MonoS column (GE Healthcare). For use in binding and structural experiments, the same sequence with an N-terminal 6-His tag and a TEV cleavage site was subcloned by recombination into the Gateway pDEST17 vector (Invitrogen). The recombinant protein was produced in Rosetta(DE3)pLysS *E. coli* strains and purified by nickel-affinity chromatography followed by cleavage using TEV protease, followed by a second nickel-affinity chromatography to remove the recombinant TEV protease and then a final gel filtration step using a Superdex 200 16/600 (GE Healthcare) equilibrated with buffer (10 mM Hepes pH 7.5 and 500 mM NaCl). For pull-down experiments, EFA6A$^{PH\text{-}Ct}$ was fused to GST and purified from bacteria according to the manufacturer's instructions (GE Healthcare). After elution with glutathione, the purified proteins were dialyzed against 20 mM Tris·HCl pH 8.0, 100 mM NaCl, 1 mM $MgCl_2$, 1 mM DTT, and 10% glycerol (dialysis buffer), and then stored at –20 °C.

Determination of k_{obs} from Initial Velocities. For EFA6$^{Sec7\text{-}PH\text{-}Ct}$ and ^{myr}Arf6, initial velocities v_i ($\Delta F_{340nm}.s^{-1}$) were determined and transformed into k_{obs} (s^{-1}) using a $\Delta\varepsilon$ value ($mM^{-1}.cm^{-1}$) calculated for each independent experiment from the ΔF_{max} and the concentration of ^{myr}Arf6.

1. Padovani D, Zeghouf M, Traverso JA, Giglione C, Cherfils J (2013) High yield production of myristoylated Arf6 small GTPase by recombinant N-myristoyl transferase. *Small GTPases* 4(1):3–8.

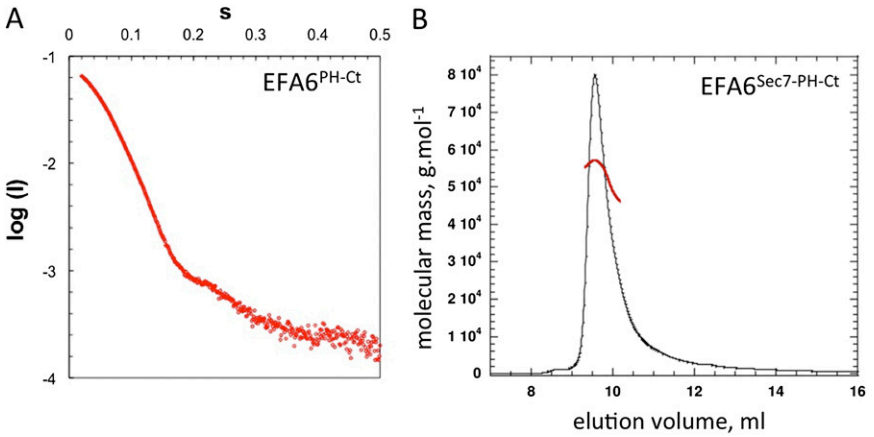

Fig. S1. Characterization of purified recombinant EFA6 constructs. (*A*) Synchrotron small-angle X-ray scattering (SAXS) analysis of EFA6$^{PH\text{-}Ct}$ from which the histidine tag has been cleaved. SAXS data were analyzed with FOXTROT software, yielding a radius of gyration of 24 Å, in agreement with an association of the PH and Ct domains in an essentially globular structure. (*B*) Size-exclusion profile (monitored by refractometry; dark lines) and the molecular masses (calculated from light-scattering and refractometry data; red lines) of EFA6$^{Sec7\text{-}PH\text{-}Ct}$. This analysis yielded a molecular mass of 57.2 ± 0.3 kDa (Rh = 3.46 ± 0.25 nm).

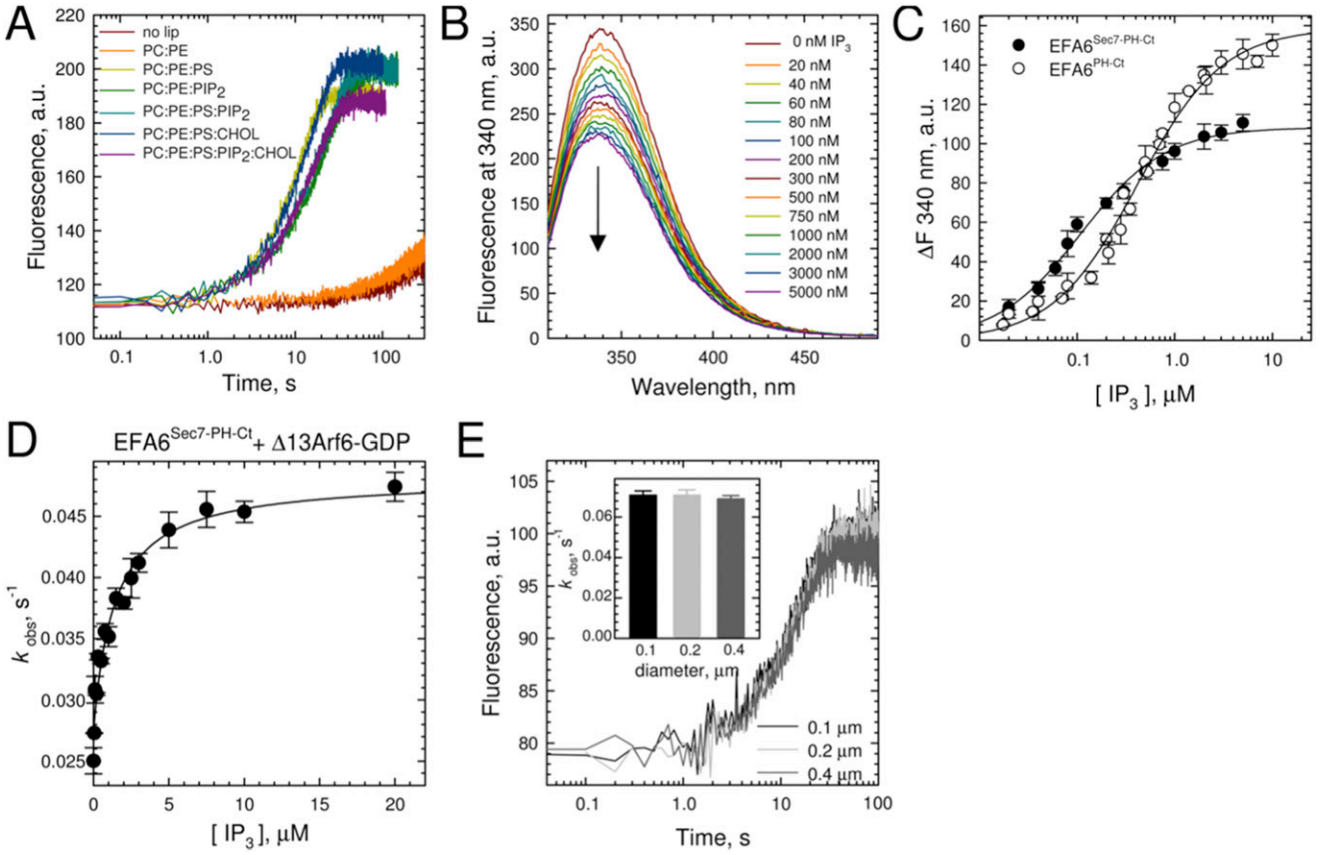

Fig. S2. Sensitivity of EFA6 to membrane composition and curvature. (*A*) Representative kinetic traces observed for the GDP/GTP exchange of ^{myr}Arf6-GDP in the presence of EFA6$^{Sec7\text{-}PH\text{-}Ct}$ on liposomes of various compositions (given in Table S1). (*B*) Fluorescence emission spectra (λ_{exc} = 280 nm) of EFA6$^{Sec7\text{-}PH\text{-}Ct}$ (1 μM) recorded in HKM buffer supplemented with 1 mM DTT at 20 °C in the presence of increasing concentrations of IP_3 (up to 5 μM). The addition of IP_3 induced a quenching of fluorescence as well as a slight red shift. (*C*) Equilibrium binding constant of IP_3 for EFA6$^{Sec7\text{-}PH\text{-}Ct}$ and EFA6$^{PH\text{-}Ct}$ determined by fluorescence. K_D values are 109 ± 9 nM and 417 ± 24 nM, respectively. (*D*) Effect of IP_3 on the EFA6$^{Sec7\text{-}PH\text{-}Ct}$-catalyzed exchange reaction of Δ13Arf6-GDP in solution. A hyperbolic fit to the data gave k_{act} (IP_3) = 1.40 ± 0.30 μM at 37 °C. (*E*) The EFA6$^{Sec7\text{-}PH\text{-}Ct}$-catalyzed exchange reaction of ^{myr}Arf6-GDP is not sensitive to membrane curvature. The diameter of liposomes is indicated.

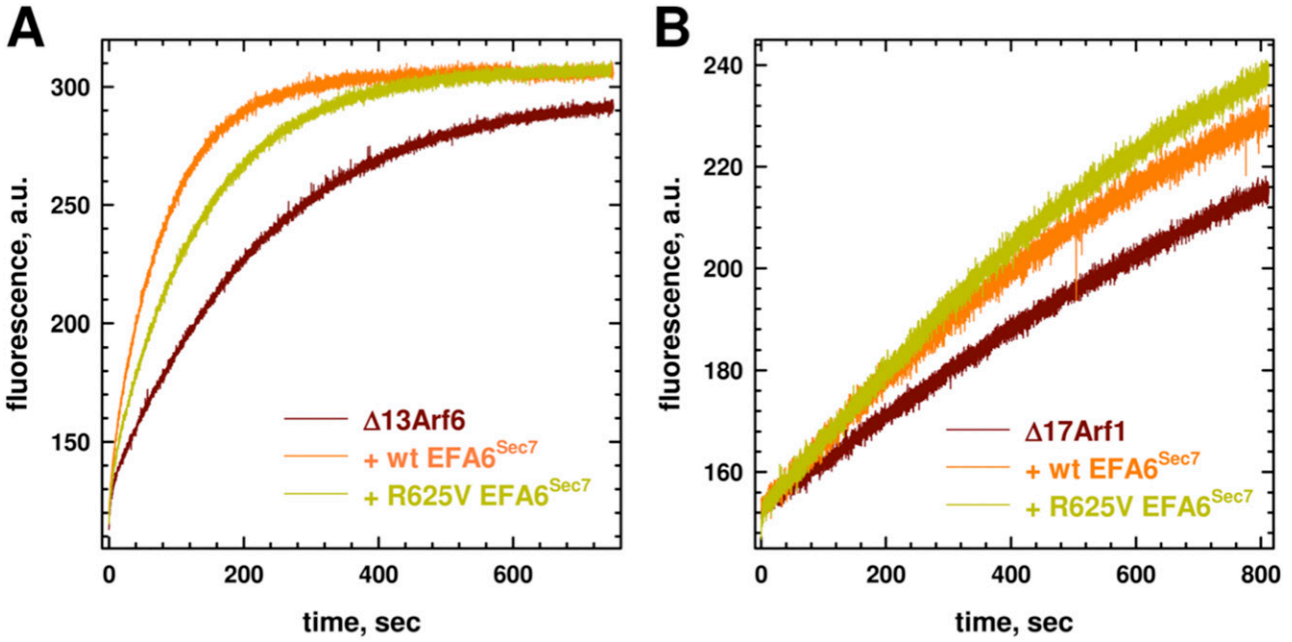

Fig. S3. Effect of the Arg625Val mutation on EFA6^{Sec7} catalytic activity. Representative kinetic traces observed for the GDP/GTP exchange reaction of 1 μM Δ13Arf6-GDP (*A*) or Δ17Arf1-GDP (*B*) alone or in the presence of EFA6^{Sec7} or EFA6$^{Sec7\text{-}R625V}$ (400 nM in *A*, 1 μM in *B*). k_{obs} values (s^{-1}) for Δ13Arf6 are 0.0043 for spontaneous, 0.0117 for EFA6^{Sec7}, and 0.0073 for EFA6$^{Sec7\text{-}R625V}$. k_{obs} values for Δ17Arf1 are 0.0007 for spontaneous, 0.0011 for EFA6^{Sec7}, and 0.0011 for EFA6$^{Sec7\text{-}R625V}$.

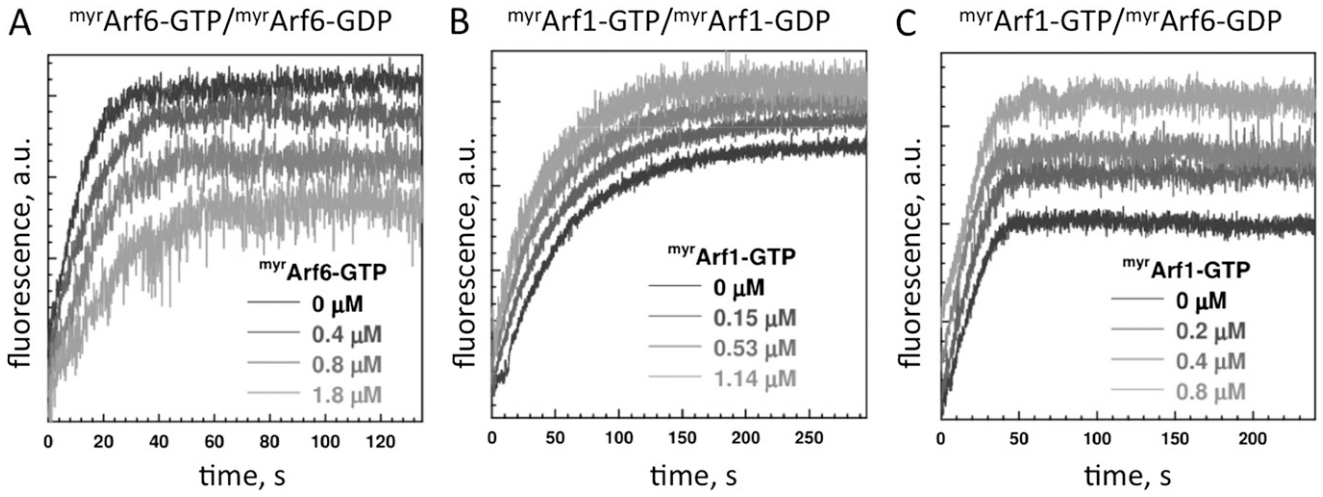

Fig. S4. EFA6 discriminates between Arf1-GTP and Arf6-GTP as effectors of the negative feedback loop. Kinetics experiments were carried out as described in Fig. 2*A*. The second part of the reaction is aligned as in Fig. 2*B*. The different ^{myr}Arf-GTP/^{myr}Arf-GDP combinations are indicated.

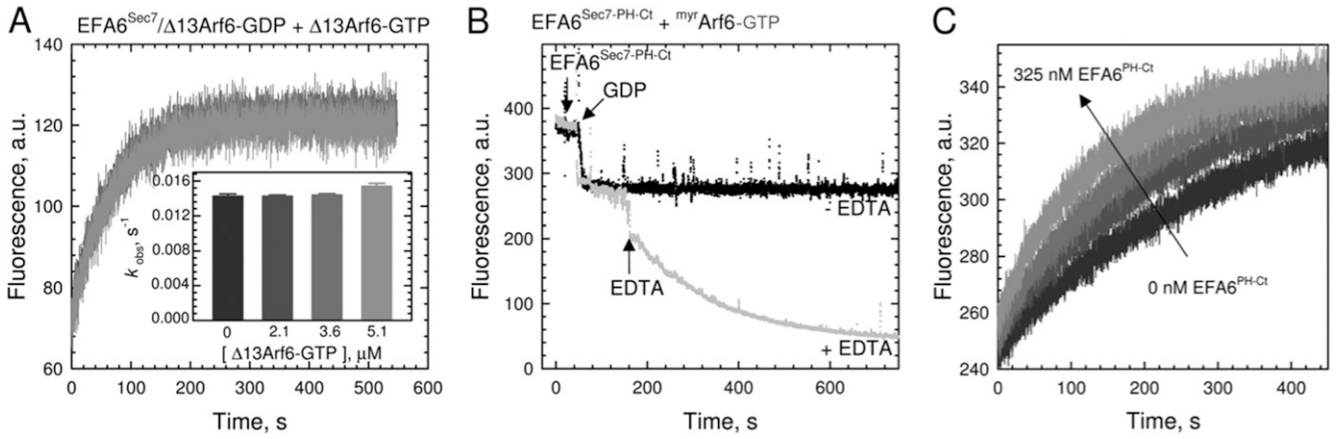

Fig. S5. Mechanism of EFA6 regulation by Arf6-GTP. (*A*) Δ13Arf6-GTP does not compete with Δ13Arf6-GDP. EFA6^{Sec7} (500 nM) exchange activity on Δ13Arf6-GDP (0.7 μM) was monitored in the presence of increasing concentrations of Δ13Arf6-GTP (up to 5.1 μM). The absence of effect indicates that the negative feedback loop does not result from a competition mechanism. (*B*) ^{myr}Arf6-GTP is not a substrate of EFA6$^{Sec7\text{-}PH\text{-}Ct}$. EFA6$^{Sec7\text{-}PH\text{-}Ct}$ (20 nM) does not stimulate the exchange of GTP for GDP from ^{myr}Arf6-GTP (0.4 μM). GTP-GDP exchange in the presence of 1 mM EDTA (no EFA6) is shown for comparison. (*C*) EFA6$^{PH\text{-}Ct}$ reverses the negative feedback effect in a dose-dependent manner. Nucleotide exchange experiments were carried out with EFA6$^{Sec7\text{-}PH\text{-}Ct}$, ^{myr}Arf6-GDP, and liposomes in the presence of increasing concentrations of EFA6$^{PH\text{-}Ct}$.

Table S1. Sensitivity of EFA6$^{Sec7\text{-}PH\text{-}Ct}$ to liposome composition

	^{myr}Arf6-GDP		^{myr}Arf1-GDP	
Liposome	k_{obs}, s^{-1}	Fold increase	k_{obs}, s^{-1}	Fold increase
None	0.00135 ± 0.00090	1	0.00037 ± 0.00012	1
PC:PE	0.00477 ± 0.00015	3.5	0.00094 ± 0.00006	2.6
PC:PE:PS	0.1275 ± 0.0162	95	0.0960 ± 0.0057	260
PC:PE:PIP_2	0.0518 ± 0.0041	38	0.0580 ± 0.0015	157
PC:PE:PS:PIP_2	0.0650 ± 0.0039	48	0.0230 ± 0.0014	62
PC:PE:PS:CHOL	0.0990 ± 0.0087	73	0.0598 ± 0.0027	162
PC:PE:PS:PIP_2:CHOL	0.0789 ± 0.0065	59	0.0275 ± 0.0014	75

CHOL, cholesterol.

Experiments were carried out using 0.4 μM ^{myr}Arf6-GDP and 11 nM EFA6$^{Sec7\text{-}PH\text{-}Ct}$ or 0.4 μM ^{myr}Arf1-GDP and 13 nM EFA6$^{Sec7\text{-}PH\text{-}Ct}$. All values are the average ± SD of three independent experiments. The lipid composition of the liposomes is as follows (% total lipids): PC:PE, PC 80, PE 20; PC:PE:PS, PC 50, PE 20, PS 30; PC:PE:PIP_2, PC 78, PE 20, PIP_2 2; PC:PE:PS:PIP_2, PC 48, PE 20, PS 30, PIP_2 2; PC:PE:PS:CHOL, PC 35, PE 14, PS 21, CHOL 30; PC:PE:PS:PIP_2:CHOL, PC 34.3, PE 14, PS 21, PIP_2 0.7, CHOL 30.